Key Points:
- Interchange injections, identified from an automated detection method, shows strongest organization in local time compared to longitude
- Longitude system dependence of equatorial interchange injections exists, but it is weak and inconsistent to previous works
- Interchange occurrence rates weakly peak at ~90° in northern SLS-5 and PPO between 7 and 9 Saturn Radii but occur at all longitudes and seasons

Correspondence to:
A. R. Azari,
azari@umich.edu

Are Saturn's Interchange Injections Organized by Rotational Longitude?

A. R. Azari[1] iD, **X. Jia**[1] iD, **M. W. Liemohn**[1] iD, **G. B. Hospodarsky**[2] iD, **G. Provan**[3] iD, **S.-Y. Ye**[2] iD, **S. W. H. Cowley**[3] iD, **C. Paranicas**[4] iD, **N. Sergis**[5,6] iD, **A. M. Rymer**[4] iD, **M. F. Thomsen**[7] iD, and **D. G. Mitchell**[4] iD

[1]Department of Climate and Space Sciences and Engineering, University of Michigan, Ann Arbor, MI, USA, [2]Department of Physics and Astronomy, University of Iowa, Iowa City, IA, USA, [3]Department of Physics and Astronomy, University of Leicester, Leicester, UK, [4]The Johns Hopkins University Applied Physics Laboratory, Laurel, MD, USA, [5]Office of Space Research and Technology, Academy of Athens, Athens, Greece, [6]Institute for Astronomy, Astrophysics, Space Applications, and Remote Sensing, National Observatory of Athens, Athens, Greece, [7]Planetary Science Institute, Tucson, AZ, USA

Abstract Saturn's magnetosphere has been extensively studied over the past 13 years with the now retired Cassini mission. Periodic modulations in a variety of magnetospheric phenomena have been observed at periods close to those associated with the emission intensity of Saturn kilometric radiation (SKR). Resulting from Rayleigh-Taylor like plasma instabilities, interchange is believed to be the main plasma transport process in Saturn's inner to middle magnetosphere. Here we examine the organization of equatorially observed interchange events identified based on high-energy (3–22 keV) H^+ intensifications by several longitude systems that have been derived from different types of measurements. The main question of interest here is as follows: Do interchange injections undergo periodicities similar to the Saturn kilometric radiation or other magnetospheric phenomena? We find that interchange shows enhanced occurrence rates in the northern longitude systems between 30° and 120°, particularly between 7 and 9 Saturn Radii. However, this modulation is small compared to the organization by local time. Additionally, this organization is weak and inconsistent with previous findings based on data with a limited time span.

Plain Language Summary When estimating the rotation rate of Jupiter and Saturn, scientists often use a periodic signal of radio emission from the planet's auroral region. At Saturn this emission is called the Saturn kilometric radiation (SKR), and unlike Jupiter, the period of SKR is observed to vary over time. Similar periodic variations have also been observed in particle energy and magnetic fields, suggesting that this periodicity is a fundamental property of the Saturn space environment. In this work, we ask if these same repetitions can be seen in a process called interchange injection. To do this, we analyze interchange's occurrence rate, as observed in particle data from the Cassini spacecraft, with respect to two longitude systems previously derived from the observed periods of the SKR emission. We find that interchange occurrence shows only weak organization in these longitude systems as compared to organization by local time.

1. Introduction

The rotation rates of gas giant planets, such as Jupiter or Saturn, cannot be determined by tracking surface features; instead, periodic variations in the emission strength within the radio frequency band are used. Saturn's rotation rate has proven to be a difficult value to definitively quantify. Estimations of the period of Saturn's kilometric radiation (SKR) have shifted significantly from the Voyager era (10 hr 39 min 24 s ± 7 s), to Ulysses (10 hr 42 min 34.2 s), and finally to Cassini (10 hr 45 min 45 ± 36 s; Desch & Kaiser, 1981; Galopeau & Lecacheux, 2000; Gurnett et al., 2005). The observed shifts in the SKR derived period are too large to represent changes in the rotation rate of the planetary body itself and must be produced by some other process yet undetermined (e.g., Cecconi & Zarka, 2005; Galopeau & Lecacheux, 2000; Stevenson, 2006). Further, adding to the mystery of Saturn's rotational period, the periodic nature of SKR is also observed throughout the magnetosphere in a range of plasma and magnetic field phenomena, including magnetic field perturbations near the equator and at high-latitudes, spoke formation in the rings, plasma density and pressure variations in the inner and middle magnetosphere, fluxes of energetic particles and energetic neutral atoms, the intensity of auroral hiss emissions, and location of the auroral oval (e.g.,

Carbary & Mitchell, 2013; Carbary et al., 2007; Gurnett et al., 2007; Gurnett, Lecacheux, et al., 2009; Gurnett, Persoon, et al., 2009; Nichols et al., 2010; Paranicas et al., 2005; Porco & Danielson, 1982; Provan et al., 2012; Ramer et al., 2017; S. Y. Ye et al., 2016). As the magnetic dipole and planetary spin axes are nearly aligned at less than 0.01° (Dougherty et al., 2018), the origin of these periodicities cannot be produced by a wobbling internal dipole as the planet rotates, as is the case for Jupiter. Many models have been proposed to explain the observed periodicities, including models that attribute the origin to processes occurring in the equatorial magnetosphere (e.g., Goldreich & Farmer, 2007; Gurnett et al., 2007; Khurana et al., 2009) and those that place the origin in the high-latitude atmosphere/ionosphere (e.g., Hunt et al., 2014; Jia et al., 2012; Smith, 2006; Southwood & Cowley, 2014). A model that incorporates flow vortices in the upper atmosphere/ionosphere has been demonstrated to be able to account for many of the observed periodic phenomena with quantitative fidelity (e.g., Jia & Kivelson, 2012; Jia et al., 2012).

For comparison, the rotation rate of Jupiter is relatively straightforward. Ground-based radio astronomers discovered and used periodic intensifications in the decametric radio frequency signals to determine a rotational rate of the planetary body itself of slightly less than 10 hr (Douglas, 1960; Franklin & Burke, 1958; Shain, 1955). The commonly used sidereal period, adopted by the International Astronomical Union, is 9 hr 55 min 29.7 s $\pm$ 0.04 s as discussed by Duncan (1975) and Seidelmann and Divine (1977). Subsequent work found the improvements from in situ measurements, for example, of the magnetic field, to be within expected error of this original estimation, and at this time there is good confidence in the rotational period of Jupiter (Yu & Russell, 2009).

Constraining Saturn's variable rotation rate is not so straightforward. In the course of this effort, magnetospheric processes have been linked to Saturn's variable planetary period, including coupling processes between the inner and outer magnetosphere. Given that many magnetospheric phenomena exhibit periodic variations, it is of particular interest to find out whether or not interchange also undergoes any periodic modulations in its occurrence rate. Similar to a Rayleigh-Taylor instability, centrifugally driven interchange is believed to be the primary process for plasma transport in the inner to middle magnetosphere (~5–12 R_s) at Saturn (see Thomsen, 2013, for a review). Associated with the interchange process are injections of hot plasma from the middle into inner magnetosphere, which are often termed interchange injections. Interchange injections are typically characterized by an enhancement of energetic (>100 eV) plasma and a depletion of low-energy plasma along with enhanced wave activity and magnetic field pressure (e.g., André et al., 2005, 2007; Azari et al., 2018; Burch et al., 2005; Chen & Hill, 2008; Hill et al., 2005; Kennelly et al., 2013; Lai et al., 2016; Rymer et al., 2009). Within this very same spatial region in which interchange is occurring, modulations of the field and plasma conditions have been observed associated with rotational periodicities (e.g., Ramer et al., 2017). Are interchange injections similarly modulated with rotational periodicities?

A previous effort by Kennelly et al. (2013) investigated this question. They analyzed data from the Cassini Radio and Plasma Wave Science (RPWS) instrument for the first half of the mission (2004–2011) to identify interchange injection events based on the presence of strong upper hybrid emissions along with the lowering of the emission frequency. The authors investigated the occurrence rate of interchange injections identified in RPWS data as a function of the northern and southern phases of the Saturn Longitude System 4 (SLS-4). In SLS-4, there is a northern and southern phase system as the SKR periods was shown to have two components, corresponding to the northern and southern auroral regions (Gurnett, Lecacheux, et al., 2009; Gurnett, Persoon, et al., 2009). Since this discovery, derived longitude systems have a northern and southern component, which differ in their period.

Kennelly et al. (2013) found a rather broad peak in the fresh interchange occurrence rate between local times of ~19 and 03 LT with a secondary narrower peak between ~12 and 17 LT. Furthermore, in the local time sector of 19 to 03, interchange was organized by the northern SLS-4 system for the pre equinox interval (i.e., prior to August 2009) and by the southern SLS-4 system in the post equinox interval. Theoretical work has tied the growth rate of interchange to ionospheric conductivity, wherein a larger conductivity suppresses interchange growth (Southwood & Kivelson, 1989). Kennelly et al. (2013) proposed that due to the seasonal differences in polar illumination, the conductivity changes drive the organization of interchange occurrence rates as organized by SLS-4. However, it is important to note that this result was obtained for the RPWS events through imposing a local time filter between 19 and 03 LT, omitting any injections at other local

times. Such a result implies the requirement of a conductivity anomaly in each hemisphere that is fixed in longitude. Prior to this work, Chen et al. (2010) found no systematic organization of interchange identified through Cassini Plasma Spectrometer data by SLS-3 (Kurth et al., 2008). However, the SLS-3 system was not defined separately for each hemisphere.

At the time of the Kennelly et al. (2013) work, the SLS-4 longitude system covered unequal time periods for the northern and southern components. Specifically SLS-4 north was defined from April 5th, 2006 to September 16th, 2009, and SLS-4 south from September 2nd, 2004 to January 9th, 2011 for (Gurnett et al., 2011). The SKR-based system has recently been updated to a SLS-5 longitude system with complete Cassini-mission temporal coverage (Ye et al., 2018). In addition, a longitude system termed the planetary period oscillation (PPO) system has been derived and continuously developed since the observation of these periodicities (see Andrews et al., 2012; Provan et al., 2013; Provan et al., 2014, for detailed process on deriving PPO properties). The PPO system is based off the analysis of the magnetic field perturbations and has also yielded phases systems and periods that now extend to the end of the Cassini mission (e.g., Provan et al., 2018, and references within). These magnetic field perturbations are quasi-sinusoidal oscillations in the magnetic field components that are periodic and closely related to the phase of SKR modulations (Andrews et al., 2008; Provan et al., 2009). It has been shown that both the SKR- and PPO-derived periods are very similar, but with some short intervals of deviation (e.g., Cowley & Provan, 2016; Fischer et al., 2015; Provan et al., 2016, 2014). Further analysis has associated periodicities in PPO with field-aligned currents flowing from Saturn's ionosphere through the magnetosphere (Hunt et al., 2014, 2015; Jia et al., 2012; Jia & Kivelson, 2012; Ramer et al., 2017). In the PPO system ~90° north and 270° south is the location of upward field aligned currents within the ionosphere of Saturn (Hunt et al., 2014, 2015). This has been discussed as associated with an inward displacement of the current system in the equatorial plane (Hunt et al., 2015). These efforts now represent two distinct rotational systems that can be used to study the entirety of periodic modulations of the Cassini data set.

Subsequent to the work by Kennelly et al. (2013), several studies have evaluated interchange distributions at Saturn, extending to close to the end of the Cassini mission in mid-September of 2017 (Azari et al., 2018; Lai et al., 2016). Azari et al. (2018) identified interchange injection events from 2005 to 2016 using a statistics-based algorithm applied to H^+ flux intensitifications from the Magnetosphere Imaging Instrument's CHarge Energy Mass Spectrometer (CHEMS) (Krimigis et al., 2004). In their work, interchange injections were found to be both more prevalent and more intense between 7 and 9 R_s. Further, interchange events were found to be primarily on the nightside of Saturn, rather than the dayside, similar to what has been found in previous work by Kennelly et al. (2013), and consistent with the idea that the growth rate of interchange is inversely proportional to the ionospheric Pedersen conductivity as first proposed by Southwood and Kivelson (1989). In addition to the broad nightside peak, Kennelly et al. (2013) also found a dayside, post noon peak, which does not seem to fit this explanation of ionospheric conductivity. Beyond examining the local time and radial dependence of their identified injection events, Azari et al. (2018) also compared their interchange injection events found in the CHEMS data to previous interchange surveys that used different detection methods. They found only modest overlap between their high-energy ion event catalogue and prior lists, and similarly for the other lists to each other, with 26 events shared by all published surveys. The overlap with the event list identified by Kennelly et al. (2013) was somewhat better than with the sets of events identified by Chen and Hill (2008) and Lai et al. (2016). With the newly updated SLS-5 and PPO-based longitude systems and the recent updated interchange lists, it is worthwhile to investigate whether or not the observed interchange injections at Saturn exhibit organization in longitude systems developed to characterize the periodic modulations of the SKR and magnetic perturbations.

In this study, we conduct an analysis similar to that of Kennelly et al. (2013) to evaluate the dependence of interchange injection, but with events identified by Azari et al. (2018) using high-energy H^+ intensifications on the SLS-5 and PPO longitude systems. We review if previously observed modulations can be observed in high-energy H^+ intensifications by first applying the same filtering method in time and local time used previously by Kennelly et al. (2013). We then extend our analysis to the full set of available mission data. We further review organization for different seasonal time ranges to identify potential seasonal trends in the occurrence of interchange injections. As discussed, a bevy of magnetospheric phenomena have been observed to modulate with these periodic systems and within this spatial region (e.g., Ramer et al., 2017).

In addition, these modulations have been associated with current systems (e.g., Hunt et al., 2015). We ask if these modulations in the physical environement are affecting the occurrence of interchange at Saturn. If interchange injections are organized by longitude throughout the Cassini era (2004–2017), then the occurrence of interchange may be sensitive to periodicities between the inner and outer magnetosphere and a source of periodic and systematic mass transport at Saturn.

2. Methodology

We use the interchange injection events identified by Azari et al. (2018) to investigate dependence on longitude for the pre equinox, equinox, and post equinox time range. We take the pre equinox date range to be 2005–2008, equinox to be 2009–2012, and post equinox to be 2013–2016. We choose 2009 through 2012 as equinox mainly because the periods of the northern and southern SKR or PPO systems within these years are close to each other, whereas outside of these years they diverge (e.g., Lamy, 2017, Provan et al., 2016 and references within). We are interested in observing differences in northern and southern system dependency during diferent seasonal time ranges.

The interchange injection events presented in Azari et al. (2018) were selected from the entire Cassini mission's equatorial CHEMS database, using all measurements within $\pm 10°$ of the Saturn Equatorial System equator and between 5 and 12 R_s. CHEMS sorts ion flux by energy per charge range, time of flight, and total energy (Krimigis et al., 2004). As we look at equatorial orbits, we would expect organization in both the southern and northern rotational systems. Events were selected through an automated detection algorithm that takes into account radial distance, energy range, and background values to identify sudden H^+ intensifications. The algorithm was trained and tested on a subset of interchange injections identified through visual inspection and then applied to all of the Cassini CHEMS data between 2005 and 2016 to obtain the first computationally standardized and comprehensive list of interchange injection events (see Azari et al., 2018, for more details). It is important to note that some of the CHEMS events in this study overlap with those RPWS events found within Kennelly et al. (2013), even though they were identified with different instruments and selection criteria.

We use the newly developed and updated SLS-5 and PPO longitude systems to evaluate periodicity dependence (Provan et al., 2018; Ye et al., 2018). SLS-4 was the first system that separated the northern and southern signals and extended the SLS identification to early 2011 using a tracking filter (Gurnett et al., 2011). SLS-5 was derived similarly and extends past 2011. To separate the northern and southern systems, Ye et al. (2018) used the polarization of the SKR signal to separate the components. In this work we use SLS-5, which now covers the whole period of the Cassini mission (see Ye et al., 2018, for additional discussion on SLS-5 and previous SLS systems).

The PPO phase/longitude systems are developed based on Cassini measurements of the quasi-periodic magnetic perturbations. For both the northern and southern PPO systems, 0° is where the perturbation field of the quasi-uniform equatorial field points radially outward (e.g., Provan et al., 2018). The PPO phases of the northern and southern systems then increase with time at a given spatial location at their respective rates, as the systems rotate in the same sense as the planet. Both SLS-5 and PPO have been converted in our analysis to represent the phase/longitudes of the spacecraft using the methods detailed most recently in Provan et al. (2018) and Ye et al. (2018).

Several studies have undertaken comparisons between the SLS and PPO systems (e.g., Cowley & Provan, 2016; Fischer et al., 2015; Provan et al., 2016, 2014). Due to the recent advances in the development of these systems, including the update to SLS-5, we present in Figure 1 a comparison between SLS-5 and PPO phases inside of 25 R_s. We use these comparisons as a guide to interpreting the differences in interchange occurrence analyses in subsequent figures. In Figure 1, we can observe that during most of the time, the phase difference remains approximately constant, meaning closely similar periods, with actual values depending on the orientation of the magnetic systems at times of corresponding SKR maxima. During most of the interval studied, the phase difference of the northern systems is near zero, meaning the quasi-uniform field of the northern system points sunward at the times of northern SKR maximum. The phase difference of the southern systems, however, generally is ~180°, meaning that the quasi-uniform field of the southern magnetic systems points antisunward at times of southern SKR maximum. PPO and SLS-5 are derived from different
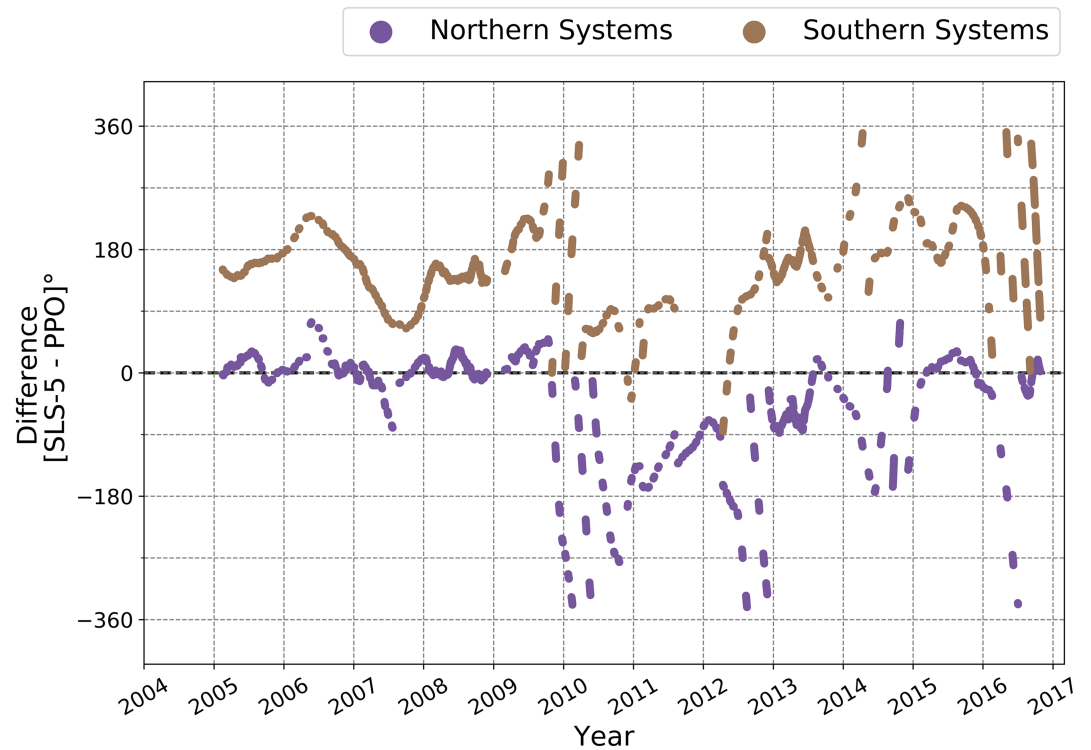
Figure 1. Difference in phase between the SLS-5 and PPO systems. The thick dashed line marks 0°, where the systems can are in phase. The difference of the northern systems is represented in purple, while southern systems are represented in a light brown.

measurements onboard the Cassini spacecraft, which helps to explain these differences. For this reason, we analyze the interchange on rotational phase using both the PPO and SLS-5 systems.

In this analysis, we focus on the locations of the interchange events as observed by Cassini, rather than backtracking them to their estimated onset locations. The events identified in the Azari et al. (2018) survey are relatively young events because the identification method was developed and optimized to avoid significant dispersion in the CHEMS energy spectra (Azari et al., 2018). Ideally, one would estimate the onset locations by accounting for the finite radial propagation time and corresponding azimuthal drift as discussed by Liu et al. (2010) and Paranicas et al. (2016). These effects would potentially affect both the local time location and the PPO and SLS-5 longitudes. Paranicas et al. (2016) estimated the radial propagation time for three dispersionless injection events. They found propagation times ranged between 1.2 and 2.4 hr. As discussed, the time an injection travels inward without showing significant dispersion governs the evolution of the injection event, but the radial velocity and starting radial distance cannot be determined independently. Paranicas et al. (2016) relied on measured phase space density using a similar methodology to Rymer et al. (2009) to obtain estimates of the starting radial distance and to derive the radiation propagation time. Paranicas et al. (2016) found a radial drift velocity ranging between ~9 and 18 km/s. The primary radial range of the interchange events found in Azari et al. (2018) is between 7 and 9 R_s. If an event onset occurs at or beyond 9 R_s, then the maximum azimuthal drift speed in this range (between 9 and 10 R_s) is ~0.69 of the rigid corotation speed with a standard error of 0.02 as estimated by Thomsen et al. (2010). Subsequent work by Wilson et al. (2017) estimated an azimuthral drift of ~0.68 between 9.5 and 10 R_s, within the error of the original work by Thomsen et al. (2010). We now estimate a maximum reasonable local time adjustment of the onset location of an interchange injection event. Taking the longer propagation time of 2.4 hr from Paranicas et al. (2016) at 0.68 of the rigid corotation velocity with a planetary rotational period of ~10.7 hr, we predict an azimuthal propagation of ~55° or of ~3.7 hr in local time. At the lower limit of the radial propagation time of 1.2 hr, at a corotation velocity of only 0.61 rigid corotation a value more representative of an onset between 12 and 13 R_s based upon Wilson et al. (2017), we would expect ~25° of azimuthal shift of observed undispersed event or <2 local time of azimuthal shift for an observed dispersionless event.

In our analysis, considering the availible data coverage, we have chosen to organize our observed interchange events in 30° longitude bins, which are larger than the lower limit of the expected aximuthal offsets between the onset and the observer location for the young injection events. We find that longitude bins of 30° present reliably consistent yet detailed results. We have also performed the statistical analysis (detailed below) with larger longitude bins but do not find any major differences in our results.

When calculating occurrence rates, we present sampling errors on all rates presented in this paper. Occurrence rates of interchange are calculated by normalizing by spatial sampling (e.g., radial location, local time, and SLS-5). More specifically, rates are calculated by taking the time Cassini spent within interchange and then dividing by the time Cassini spent in totality in that spatial region (e.g., radial location, local time, and SLS-5). This corrects for sampling bias in the Cassini orbits. We include on the occurrence rates propagated error. This is calculated from traditional propagation of error rules. The two sources of error are from the sampling error on time within interchange, and sampling error on time within spatial location, of the form $1/(\text{sample size})^{1/2}$.

3. Results and Discussion

We seek to determine whether or not interchange occurrence can be organized by either of these two longitude systems, that is, SLS-5 and PPO. In light of the previous findings of different relationships during pre equinox and post equinox (Kennelly et al., 2013), we examine the Cassini mission by analyzing the pre equinox, equinox, and post equinox time ranges separately. We begin by comparing results with the previous work by analyzing our events in SLS-5 for the same time and local time range used in Kennelly et al. (2013) (section 3.1). Section 3.1 is the only section in which we take a local time filter. We then use the updated SLS-5 and PPO systems for the whole pre equinox time range 2005–2008 (section 3.2), the equinox time range 2009–2012 (section 3.3), the post equinox 2013–2016 (section 3.4) mission interval, and all 2005–2016 equatorial data (section 3.5) without restricting by local time.

3.1. Comparison With Previous Studies With Different Sampling Constraints

We first examine the dependence of occurrence rates of the Azari et al. (2018) interchange events on the SLS-5 longitudes for the same pre equinox interval and local time range (19–03 LT) used by Kennelly et al. (2013). SLS-4 north was defined from April 5th, 2006 to September 16th, 2009, and SLS-4 south from September 2nd, 2004 to January 9th, 2011. Following Kennelly et al. (2013), who used August of 2009 as equinox, we evaluate our events in the pre equinox time range for SLS-5 north between April 5th, 2006 to August 2009 and SLS-5 south between the start of our own survey (2005) to August 2009. As a result, the total number of events available for evaluation of the northern phase becomes 100 while the southern phase event sample becomes 175. The limitation is discussed further in this section. More information on the valid date ranges for the SLS phase systems is available at the SLS-4 website (http://cassini.physics.uiowa.edu/sls4/).

As shown in Figure 2, our analysis confirms the original results of Kennelly et al. (2013) for the pre equinox time range between 19 and 03 LT. Starting with the northern system (Figure 2, upper panel), the distribution of those events shared between the lists of Kennelly et al. (2013) and Azari et al. (2018) (magenta shading) shows a strong peak within the 60–90° northern longitude bin, very similar to the previous work. Further, the distribution of high-intensity events shows a similar peak in the 30–60° longitude bin. The distribution of all events identified in the Azari et al. study exhibit two comparable peaks within a broader longitude range of ~30–180° that encompasses the peaks seen in the high-intensity events and the events shared with the Kennelly et al. study. Our full set of injection events exhibits another peak in the ~300–330° SLS-5 north longitude bin. This peak is primarily due to events found at distances greater than 11 R_s. We discuss this radial bifurcation of our peaks in section 3.4. As the Kennelly et al. (2013) events are all within 11 R_s, we do not expect to see this peak in the overlapping data set. We also performed an analysis without this local time filter and find a similar distribution to that presented in Figure 2.

The total event distribution of events as function of the SLS-5 southern longitude (lower panel of Figure 2) shows an apparent preference centered on the 0° bin ranging between 240° and 120°. An additional secondary peak is in the 210–240° range. The primary difference between the northern and southern systems in our analysis however is the nonapparent organization of the events shared between the Kennelly and Azari lists and of the high-intensity events, in which the northern system showed a singular peak and the southern
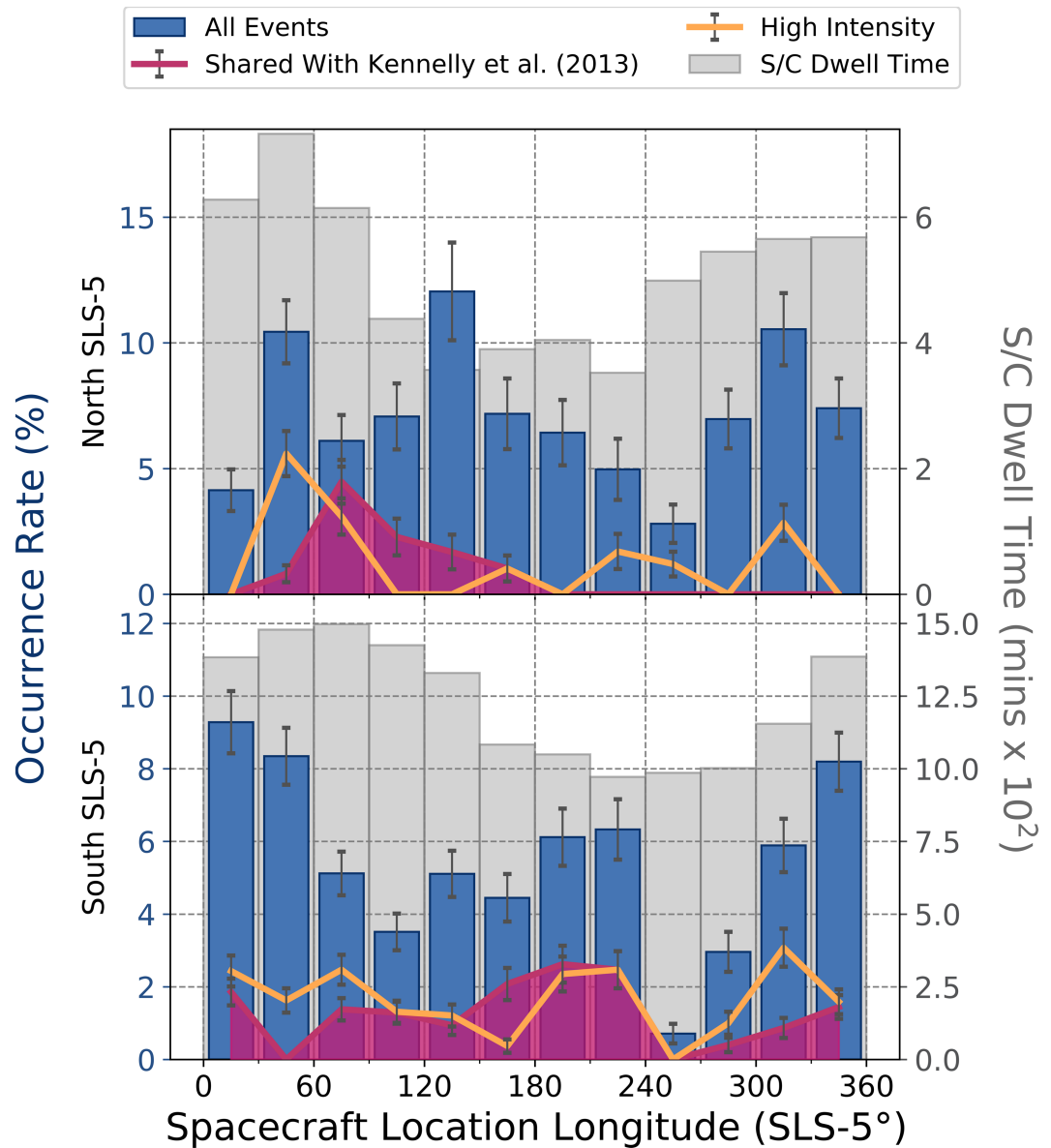
Figure 2. Pre equinox interchange injection events normalized by spacecraft dwell time in SLS-5 between 19 and 03 LT. The top chart shows the normalized distribution of interchange events in SLS-5 north between April 2006 and August 2009 while the bottom chart shows the events in SLS-5 south between January 2005 and August 2009. The error bars are representative of the sampling error of $1/(\text{sample size})^{1/2}$ on the event and dwell time and propagated appropriately. The gray-shaded bars show the total sample size. The blue bars are the interchange events identified by Azari et al. (2018). The orange line represents the extremely high H^+ flux events of Azari et al. (2018) (>3 σ above background values). The magenta-shaded region represents events found by both Kennelly et al. (2013) and Azari et al. (2018).

system has a lack of any apparent preference on a specific longitude bin. The lack of apparent organization by SLS-5 southern longitude for these high-intensity and overlap events is in agreement with the earlier results obtained by Kennelly et al. (2013). Interestingly, the distribution of all events in the Azari et al. list shows a different pattern in that there is a broad peak over the southern longitude range between 330° and 60°. However, the distribution of all events (shown in blue) for both the northern and southern SLS-5 systems shows broad peaks within this time range. We cannot claim that the all event distribution of the northern system is more or less organized than the southern system for this time range.

Let us comment on the primary differences we have observed between the northern and southern SLS-5 systems within this sampling regime. This single-peaked distribution for the northern system is seen both with

the events shared between Kennelly et al. (2013) and Azari et al. (2018) and our high-intensity events—also known as category 4 events, which have enhancements >3 standard deviations (σ) above background values in CHEMS as described in Azari et al. (2018). As can be seen in Figure 2, these two subsets of events show a similar distribution to each other. In the sections below, we use category 4 events as proxies for Kennelly et al. (2013) events, as their published list does not continue into the post-2012 date range.

As discussed above, applying the local time and time filters as required for direct comparison to previous works leads to different numbers of events for the northern and southern SLS-5 systems. There are a total of 100 events for evaluation of dependence of SLS-5 northern longitude, of which 12 events are shared with Kennelly et al. (2013) and 11 events are of high intensity. The 12 events shared with Kennelly et al. (2013) all come from just three orbits in the later half of 2007. Meanwhile, there are a total of 175 events for evaluation of dependence of SLS-5 southern longitude, of which 38 events are shared with Kennelly et al. (2013) and 30 events that are of high intensity. The 38 events shared with Kennelly et al. (2013) were observed during 12 orbits between 2005 and 2007. This difference between the northern and southern sample size is simply due to the availability of the SLS-4 system discussed above. In our analysis we used SLS-5 but did apply the same historical restrictions that previous works had using SLS-4.

Restricting the local time and time range to compare to previous works yields three times as many high-intensity events in the SLS-5 south longitude system as compared to SLS-5 north. There are also nine more orbits in the southern system events, resulting in better spatial. We are now able to confirm that the interchange events identified in the CHEMS data in SLS-5 show a single peaked distribution, primarily located in the high-intensity events. This is the very same peak that Kennelly et al. (2013) found in the pre equinox period through identifying events with RPWS.

Therefore, we find that with the same sampling and restrictions, we are able to reproduce the dependence on the northern system in the pre equinox period for high-intensity events. The southern system does show disorganized behavior in the high-intensity events, which also agrees with previous findings. However, the overall distribution of all events appear similar between the northern and southern systems. The sampling restrictions primarily affected these high-intensity events of which are most similar to previous findings. Now we move on to expanding our sampling to all local times and available years to obtain equal sampling for time range and number of events between seasonal selections to evaluate the complete pre equinox, during equinox, and post equinox time periods.

3.2. Pre Equinox Distribution

Figure 3 shows the distribution of interchange occurrence rates from 2005 to 2008 as a function of the PPO and SLS-5 longitudes. The analysis in this section is not restricted by local time. Similar to Figure 2, we plot all events or the overall distribution in dark blue. Based on Figure 3 we note that the SLS-5 north and PPO north system distributions do show similar distributions but there are also minor differences. This is to be expected because in Figure 1 we can see that between 2005 and 2008 the difference between PPO and SLS-5 north trends close to 0° with some deviations. We also note that the southern systems do show dissimilar patterns due to the offsets between these systems. As discussed previously the difference between the two southern longitude systems during the pre equinox period centers around ~180° due to the system definitions, and the distribution of injections as organized by the southern systems of SLS-5 and PPO does appear to be similar if shifted by ~180°. We can observe this most easily for the total event distribution (blue shaded bars).

As noted in section 3.1, the northern system had markedly smaller sampling than the southern system. There are 256 events represented in this figure with 47 events shared with Kennelly et al. (2013) and 43 of high H^+ flux intensity (magenta-shaded regions and orange lines, respectively). While there are subtle rises and falls in the overall distribution with longitude in all northern and southern systems, we find that by introducing larger sample sizes (which also makes them roughly equal), the stark differences seen previously in Kennelly et al. (2013) are reduced. The results presented here are not filtered by local time, but we found no significant changes in the results with local time restricted to the nightside. As discussed above, the Azari et al. (2018) events are predominantly located on the nightside, and therefore, filtering by local time only slightly reduces the sample size but does not affect the overall longitude pattern.
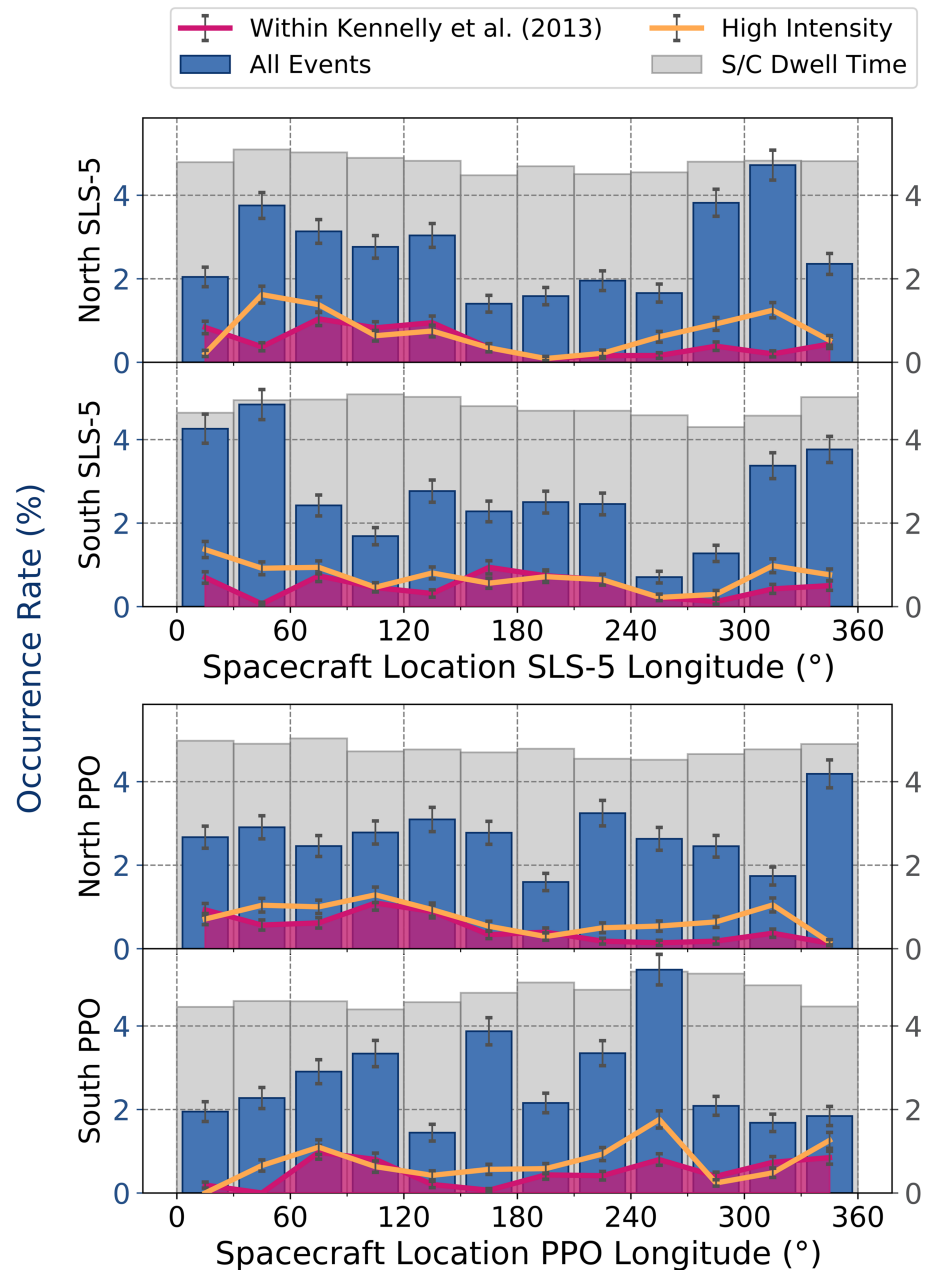
Figure 3. Interchange injection events normalized by spacecraft dwell time between 2005 and 2008 by SLS-5 and PPO. The top chart shows the normalized distribution of interchange events in SLS-5 north, followed by SLS-5 south, then PPO north, and PPO south. The error bars are representative of the sampling error of $1/(\text{sample size})^{1/2}$ on the event and dwell time and propagated appropriately. The gray-shaded bars show the total sample size. The blue bars show the interchange events identified by Azari et al. (2018). The orange line represents extremely high H^+ flux events of Azari et al. (2018) (>3 σ above background values). The magenta-shaded region represents events found within both Kennelly et al. (2013) and Azari et al. (2018).

We find peaks in the injection occurrence rate in the SLS-5 north system for both overall events and for high-intensity events: There are two peaks: one centered between 0° and 120° and another between 300° and 330°. The 0–120° peak mirrors our previous finding in section 3.1, and by expanding the sampling we pick up additional patterns at other longitudes. In the PPO system, this trend is less clear, particularly when all events are included. In the southern SLS-5 system we observe a broad peak around 0° and in the southern PPO system multiple modest peaks, but in particular at 240–270°.

The difference between the northern and the southern system is small, and we cannot claim that in the pre equinox period the northern system is more organized than the southern system. To confirm previous theories on systematic hemispheric seasonal dependence, we were expecting to observe an organization in the northern system as compared to an unorganized southern system due to differences in the dominant phase system. We have not observed a distinct change in organization with system.

In the PPO system 90° and 270° are of particular significance with respect to field aligned current systems since in the northern ionosphere parallel currents are directed outward at 90° and inward at 270° and reversed for the southern system (Hunt et al., 2014, 2015). We do observe small enhancements near these locations of interchange occurrence rates but only within the most intense of interchange events ($>3\,\sigma$ above background). We can say similarly for specific physical locations in the SLS-5 systems. These enhancements are small as compared to the values at other longitude locations and not reliably located in any singular hemisphere. We discuss this further in the following sections.

3.3. Equinox Distribution

We now analyze the equinox period between 2009 and through 2012. The analysis in this section is not restricted by local time. Figure 4 shows the occurrence rates of interchange within this period with no local time filters. There are 364 events represented in this figure with 63 events shared with Kennelly et al. (2013) and 92 of high H^+ flux intensity events. Overall, we do not observe a greater organization by the northern and the southern systems than seen in pre equinox. However, within this time range we do not expect to see great organization due to the similarity of the periods between 2010 and 2012.

In the SLS-5 charts we observe the northern system has greater occurrence rates again between 0° and 120° and around 270°. This is the same 0–120° as seen both in the subset sampling (section 3.1) and in the full pre equinox data set (section 3.2). For comparison, the northern PPO system shows peaks between 90–120° and 210–240°. Unlike the northern systems, the southern systems for both SLS-5 and PPO show distinct behavior from the pre equinox period unlike the northern systems. SLS-5 shows enhanced occurrence rates between 60–90° and 270–300°, while PPO shows enhancements around 180–210°.

Comparing the results between equinox and pre equinox, we find that the event distribution pattern in the southern system has undergone significant changes between the two seasonal phases, whereas in the northern systems interchange occurrence consistently exhibits enhancement around the ~90° phase. This is unexpected as compared to the previous work by Kennelly et al. (2013).

3.4. Post equinox Distribution

We now evaluate the post equinox distribution of interchange by longitude for 2013–2016. The analysis in this section is not restricted by local time. Similar to previous sections, we present the distribution without filtering for nightside local time in order to maximize the sample size for our statistical analysis. In Figure 5, we present 196 events from Azari et al. (2018) of which 40 are of high intensity. We do not present our results for the category of events shared with Kennelly et al. (2013) because the Kennelly survey ends within this period and there are only a handful of events (i.e., not enough for statistical significance). However, we note that as shown in Figures 2 and 3, the distribution of our identified high-intensity events is very similar to that found in the shared-event set. Indeed, over all time, the highest intensity events find greater cross-correlation between lists than weaker intensity events (Azari et al., 2018). Similar to the equinox distributions, the northern and southern systems both show differences between SLS-5 and PPO. This is not unexpected, as there are more differences in the phases between SLS and PPO in the post equinox period (see Figure 1). Within Figure 5 we continue to observe an enhancement between 30° and 120° within the northern systems, but the secondary peak has decreased. The southern systems on the other hand show a large change from the pre equinox and equinox periods, but not toward a more organized behavior as found within Kennelly et al. (2013). The post equinox phases used by Kennelly et al. (2013) was only available between August of 2009 and January 2011—whereas the post equinox period used in this work is 2013–2016 (see section 2). We expect however that if a post equinox organization of the southern system persists, it would be evident in 2013 and onward. Indeed, the peaks in the southern system are just as high,
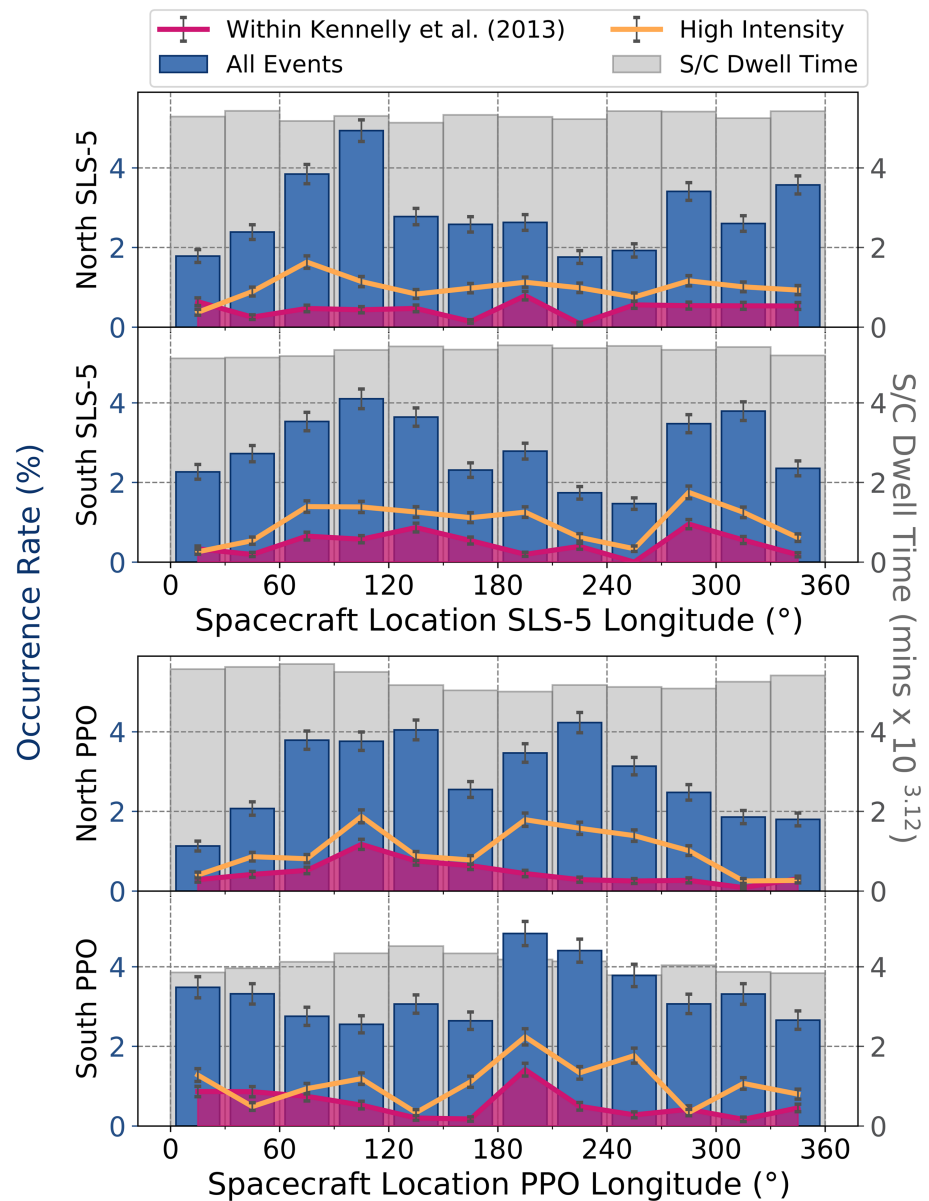
Figure 4. Interchange injection events normalized by spacecraft dwell time between 2009 and 2012 by SLS-5 and PPO. The top chart shows the normalized distribution of interchange events in SLS-5 north, followed by SLS-5 south, then PPO north, and PPO south. The error bars are representative of the sampling error of $1/(\text{sample size})^{1/2}$ on the event and dwell time and propagated appropriately. The gray-shaded bars show the total sample size. The blue bars show the interchange events identified by Azari et al. (2018). The orange line represents extremely high H^+ flux events of Azari et al. (2018) ($>3\,\sigma$ above background values). The magenta-shaded region represents events found within both Kennelly et al. (2013) and Azari et al. (2018).

and indeed, the dips just as low, but they do not cluster in a broad region, nor remain consistent between pre equinox, equinox, and post equinox time periods.

We observe that the interchange event occurrence shows persistent enhancement within the ~0–120° in the northern phase systems during the post equinox time period, just as seen in the pre equinox and equinox time periods. The distributions are dissimilar to each other between the PPO and SLS-5 southern systems —not unexpectedly from the phase differences (see Figure 1). In previous works reviewing this interchange event list, occurrence rates were strongly organized in radial distance and local time (Azari et al., 2018). In
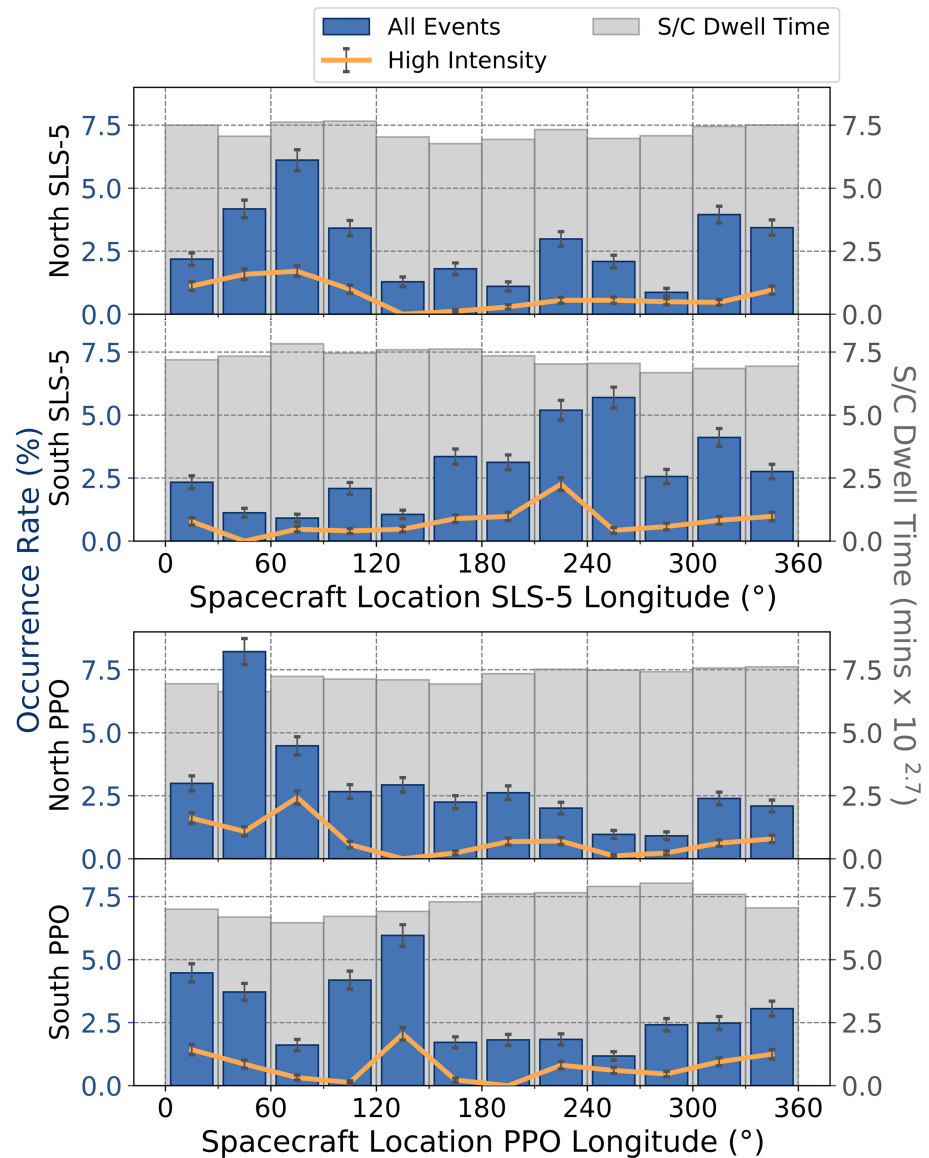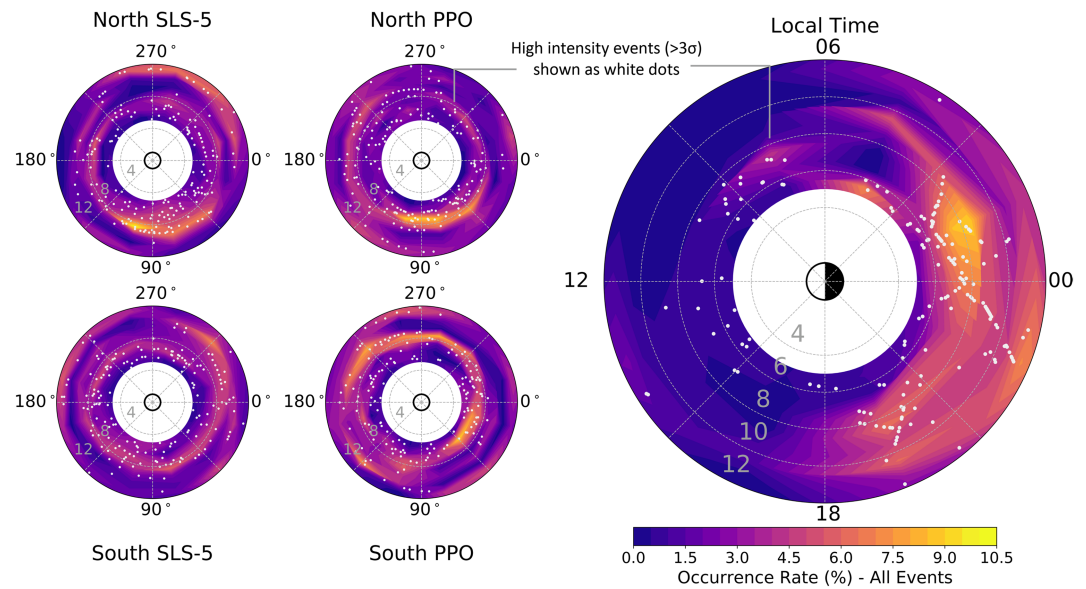
Figure 5. Interchange injection events normalized by spacecraft dwell time between 2013 and 2016 by SLS-5 and PPO longitude. The top chart shows the normalized distribution of interchange events in SLS-5 north, followed by SLS-5 south, then PPO north, and PPO south. The error bars are representative of the sampling error of $1/(\text{sample size})^{1/2}$ on the event and dwell time and propagated appropriately. The gray-shaded bars show the total sample size. The blue bars show the interchange events identified by Azari et al. (2018). The orange line represents extremely high H^{+} flux events of Azari et al. (2018) ($>3\,\sigma$ above background values).

section 3.5 we compare these statistics over all years combined as compared to local time and radial organization, having now found little difference in the northern systems with season.

3.5. Organization of Interchange Over All Years for Longitude, Local Time, and Radial Distance

Figure 6 shows the SLS-5, PPO, and radial and local time dependence of interchange occurrence rates for all the events identified in Azari et al. (2018). The right-hand panel of the figure shows the strongly nightside dominant local time organization discussed by Azari et al. (2018) with occurrence rates stronger by about 5–6 times on the nightside compared to the dayside. The left panels present the occurrence rates by rotational longitude and radial distance. In the northern systems, the small peak described within sections 3.2–3.4 between 30° and 120° clearly appears in both the SLS-5 and PPO plots. These panels all show that the injection events occur primarily near 8 R_s. The secondary peak present in the SLS-5 northern system

Figure 6. Interchange injection events normalized by spacecraft dwell time between 2009 and 2016 by SLS-5, PPO, and local time. The white dots represent extremely high H^+ flux events ($>3\,\sigma$ above background values; Azari et al., 2018). All subplots share the same color bar.

around ~300° is seen to be due to events outside of 11 R$_s$, which is outside the radial range included by Kennelly et al. (2013). This range was shown to have a larger proportion of enhancements due to tail effects (e.g., current sheet collapse) rather than interchange in the Azari et al. (2018) event list. We therefore focus on the peak located between 30° and 120° in this discussion rather than those between 11 and 12 R$_s$. As noted above, ~90° north and 270° south in the PPO system is the location of upward field aligned currents within the ionosphere of Saturn (Hunt et al., 2014, 2015). This has been discussed as associated with an inward displacement of the current system in the equatorial plane (Hunt et al., 2015). The peak in our interchange distribution might suggest that there is a systematic effect at this location, potentially because (1) changing the curvature of the magnetic field affects Rayleigh-Taylor instabilities in curved magnetic field configurations (e.g., Komori et al., 1978) and/or (2) through magnetosphere-ionosphere coupling augmenting the instability criterion. Such upward field aligned currents are often associated with increase conductivity, which based on previous models are thought to suppress interchange (Southwood & Kivelson, 1987; Southwood & Kivelson, 1989) whereas we observe an intensification in a some, but not all of the upward field aligned regions. We stress that while the peak at ~90° in the northern systems seems to persists throughout the Cassini era, the southern systems show no clear enhancement around 270°. Therefore, a switching of ionospheric control of interchange dependent on Saturnian season as observed in rotating longitude systems is inconsistent with our data analysis results.

The white scatter plot points in Figure 6 show the locations of the events of highest intensity ($>3\,\sigma$). The white dots exhibit little organization in the SLS-5 and PPO coordinate systems and instead occur at many different longitudes. According to Azari et al. (2018), these events correspond to those that are commonly shared among available surveys based on different identification methods. For a quantitative comparison, we calculate the maximum occurrence rate to minimum occurrence rate difference for SLS-5 north as compared to the same metric for local time distribution for all radial distances and years. We use SLS-5 north, as this shows the most extreme difference between the maximum and minimum values for all longitude systems.

For SLS-5 north, the peak occurrence rate over 2005–2016 occurs between 60° and 90° at 4.24% +/− 0.17% and the minimum occurs at 240–270° at 1.90% +/− 0.12%. The error calculated here is the error as described in the methodology section of propagated sampling error. At the maximum occurrence rate we therefore find an enhancement of ~2 times as compared to the minimum without overlapping error calculations. Comparatively for the local time distribution over all years, which can be observed in Azari et al. (2018) and further reviewed in this present work, the peak occurrence rate occurs between 00 and 02 local time

hours at 5.70% +/− 0.15%, and the minimum occurs between 10 and 12 LT at 0.19% +/− 0.03%. The ratio between the maximum and minimum rate is ~30. However, in our previous work we report the difference in rates as compared not to the minimum, as this value is rapidly approaching zero near noon, but the pre noon and post noon quadrants between 08–10 LT and 14–16 LT with occurrence rates of 0.95% +/− 0.07% and 1.07 +/− 0.08%, respectively. This results in a rate enhancement of ~5–6 times.

The radial location and local time distribution have been extensively discussed in Azari et al. (2018). The predominant peak around 7–9 R_s has been attributed to the competition between energization of inward bound injections and charge-exchange losses. The dominant nightside occurrence rates are in good agreement with the local time distribution of suprathermal particles in the inner to middle magnetosphere (e.g., Sergis et al., 2017; Thomsen et al., 2016). This is consistent with interchange as a primary radial transport mechanism additionally discussed by Dejong et al. (2010) and Hill (2016). Examining the combined local time and radial distribution in Figure 6, we note a nightside asymmetry wherein the peak interchange occurrence rates are on the postmidnight rather than premidnight local time region, suggesting the triggering mechanisms of interchange is primarily intensified on the nightside, perhaps by large-scale tail injections or current sheet collapse. That is, large-scale tail injections form a fresh population of ~keV ions just beyond 10 R_s in the midnight local time region. As these particles will drift eastward toward the dawn sector, there is a higher likelihood of interchange injection in the postmidnight region, as seen in the right-hand panel of Figure 6.

The longitude enhancement is weak as compared to the local time enhancement. In addition, the northern system shows consistent enhancement, which does not change with season, and the southern system varies with season but not in a systematic manner. This is inconsistent with previous works and does not agree with current findings of interchange as responsive to seasonal differences in planetary period determinations. Instead, we interpret this result to suggest that the primary mechanisms behind interchange instability are strongly dependent on local time, with a weak enhancement due to physical mechanisms in the rotational phase systems.

4. Conclusion and Outstanding Questions

The dependence of the occurrence rates of interchange events identified by Azari et al. (2018) have been examined as a function of radial distance, local time, SLS-5 longitudes (north and south), PPO longitudes (north and south), and seasonal phases. Separate analyses were done for the full set of events and for the subsets of highest-intensity events (>3 σ above background of CHEMS) and events found also in a previous survey (Kennelly et al., 2013).

Within the same local time and date range examined by Kennelly et al. (2013), there is a distinct peak within the 30–120° range of SLS-5 north. This confirms their results, which were based on SLS-4 of an organized pre equinox system. However, with a larger sample size the distribution shows additionally patterns at other longitudes in the northern system, and this peak diminishes, becoming comparable to the patterns in the southern SLS-5 system. Further, we find that the northern longitude systems continue to show this 30–120° enhancement for the equinox and post equinox time ranges. The results of Kennelly et al. (2013) suggest that this should not be the case, instead shifting to dominance by the southern longitude systems after equinox. This location of enhancement also shows distinct radial preference, located at ~ 8 R_s, within the peak occurrence range of interchange injections at Saturn between 7 and 9 R_s (Azari et al., 2018). Our results show that interchange occurrence rates are not located in a singular longitude location by hemisphere or otherwise.

We find that there is a factor-of-2 increase in occurrence at peak locations between 30° and 120° in the northern SLS-5 and PPO systems. We compare this to the enhancement found by Azari et al. (2018), which examined the local time distribution and found an enhancment of ~ 5–6 times on the nighside as compared to the dayside. We further identify an asymmetry on the nightside, where peak interchange rates occur in the postmidnight rather than the premidnight sector, suggesting triggering mechanisms of interchange is primarily intensified on the nightside, perhaps by large-scale tail injections or current sheet collapse.

The rather weak correlation between interchange occurrence and longitude systems suggests that rotational periodicities do not represent a primary mechanism influencing interchange injections. It is, however, possible that periodicities and their causation can contribute through secondary effects such as the physical

properties of interchange injection events (overall mass and energy transfer) or through other, still unexplored mechanisms in the middle magnetosphere of Saturn. Future work should consider investigation of solar influence on ionospheric conductivity through solar ultraviolet irradiance on the modulation of the occurrence rate of interchange as ultraviolet has been observed to affect the energetic environment (e.g., Kollmann et al., 2017; Roussos et al., 2014). We also note that interchange events used in this work are equatorial and subsequent work should additionally review high inclination injections for dependencies. The dependencies found in the present study do not totally preclude ionospheric control of interchange, but they show it to be at best a fairly weak influence.

Our results raise several questions in regard to interchange injection events. In particular, if such organization is found in the northern systems (PPO and SLS-5), why is there no such equivalent in the southern system for equatorial events? Why does the 90° peak in the northern longitude system persist through all the seasons sampled? Additionally, these events studied were identified based on enhanced fluxes of high-energy ions, would interchange events identified using other instruments on-board Cassini show similar results? As shown by Azari et al. (2018), there are major differences in interchange surveys, and such efforts should be undertaken to continue identifying interchange injections in Cassini data. Future work should also investigate if interchange at Jupiter has any potential dependence on local time, radial distance, or longitude. As a gas giant with a similar mass transfer process, such a study would be essential in piecing together how rotational effects might affect the interchange process at rapidly rotating systems.

References

André, N., Dougherty, M. K., Russell, C. T., Leisner, J. S., & Khurana, K. K. (2005). Dynamics of the Saturnian inner magnetosphere: First inferences from the Cassini magnetometers about small-scale plasma transport in the magnetosphere. *Geophysical Research Letters*, *32*, L14S06. https://doi.org/10.1029/2005GL022643

André, N., Persoon, A. M., Goldstein, J., Burch, J. L., Louarn, P., Lewis, G. R., et al. (2007). Magnetic signatures of plasma-depleted flux tubes in the Saturnian inner magnetosphere. *Geophysical Research Letters*, *34*, L14108. https://doi.org/10.1029/2007GL030374

Andrews, D. J., Bunce, E. J., Cowley, S. W. H., Dougherty, M. K., Provan, G., & Southwood, D. J. (2008). Planetary period oscillations in Saturn's magnetosphere: Phase relation of equatorial magnetic field oscillations and Saturn kilometric radiation modulation. *Journal of Geophysical Research*, *113*, A09205. https://doi.org/10.1029/2007JA012937

Andrews, D. J., Cowley, S. W. H., Dougherty, M. K., Lamy, L., Provan, G., & Southwood, D. J. (2012). Planetary period oscillations in Saturn's magnetosphere: Evolution of magnetic oscillation properties from southern summer to post-equinox. *Journal of Geophysical Research*, *117*, A04224. https://doi.org/10.1029/2011JA017444

Azari, A. R., Liemohn, M. W., Jia, X., Thomsen, M. F., Mitchell, D. G., Sergis, N., et al. (2018). Interchange injections at Saturn: Statistical survey of energetic H+ sudden flux intensifications. *Journal of Geophysical Research: Space Physics*, *123*, 4692–4711. https://doi.org/10.1029/2018JA025391

Burch, J. L., Goldstein, J., Hill, T. W., Young, D. T., Crary, F. J., & Coates, a. J., ... Sittler, E. C. (2005). Properties of local plasma injections in Saturn's magnetosphere. *Geophysical Research Letters*, *32*, L14S02. https://doi.org/10.1029/2005GL022611

Carbary, J. F., & Mitchell, D. G. (2013). Periodicities in Saturn's magnetosphere. *Reviews of Geophysics*, *51*, 1–30. https://doi.org/10.1002/rog.20006

Carbary, J. F., Mitchell, D. G., Krimigis, S. M., & Krupp, N. (2007). Electron periodicities in Saturn's outer magnetosphere. *Journal of Geophysical Research*, *112*, A03206. https://doi.org/10.1029/2006JA012077

Cecconi, B., & Zarka, P. (2005). Model of a variable radio period for Saturn. *Journal of Geophysical Research*, *110*, A12203. https://doi.org/10.1029/2005JA011085

Chen, Y., & Hill, T. W. (2008). Statistical analysis of injection/dispersion events in Saturn's inner magnetosphere. *Journal of Geophysical Research*, *113*, A07215. https://doi.org/10.1029/2008JA013166

Chen, Y., Hill, T. W., Rymer, A. M., & Wilson, R. J. (2010). Rate of radial transport of plasma in Saturn's inner magnetosphere. *Journal of Geophysical Research*, *115*, A10211. https://doi.org/10.1029/2010JA015412

Cowley, S. W. H., & Provan, G. (2016). Planetary period oscillations in Saturn's magnetosphere: Further comments on the relationship between post-equinox properties deduced from magnetic field and Saturn kilometric radiation measurements. *Icarus*, *272*, 258–276. https://doi.org/10.1016/j.icarus.2016.02.051

Dejong, A. D., Burch, J. L., Goldstein, J., Coates, A. J., & Young, D. T. (2010). Low-energy electrons in Saturn's inner magnetosphere and their role in interchange injections. *Journal of Geophysical Research*, *115*, A10229. https://doi.org/10.1029/2010JA015510

Desch, M. D., & Kaiser, M. L. (1981). Voyager measurement of the rotation period of Saturn's magnetic field. *Geophysical Research Letters*, *8*(3), 253–256. https://doi.org/10.1029/GL008i003p00253

Dougherty, M. K., Cao, H., Khurana, K. K., Hunt, G. J., Provan, G., Kellock, S., et al. (2018). Saturn's magnetic field revealed by the Cassini Grand Finale. *Science*, *362*(6410), eaat5434. https://doi.org/10.1126/science.aat5434

Douglas, J. N. (1960). A study of non-thermal radio emission from Jupiter. H.D. Dissertation, Yale University, New Haven, 1962–1963. Retrieved from http://search.proquest.com/docview/302239822/citation/9F7E6667508A4F0DPQ/3?accountid=28962

Duncan, R. A. (1975). Jupiter's rotation period from dekametric observations 1951–1975. *Publications of the Astronomical Society of Australia*, *2*(06), 342–345. https://doi.org/10.1017/S1323358000014211

Fischer, G., Gurnett, D. A., Kurth, W. S., Ye, S. Y., & Groene, J. B. (2015). Saturn kilometric radiation periodicity after equinox. *Icarus*, *254*, 72–91. https://doi.org/10.1016/j.icarus.2015.03.014

Franklin, K. L., & Burke, B. F. (1958). Radio observations of the planet Jupiter. *Journal of Geophysical Research*, *63*(4), 807–824. https://doi.org/10.1029/JZ063i004p00807

Galopeau, P. H. M., & Lecacheux, A. (2000). Variations of Saturn's radio rotation period measured at kilometer wavelengths. *Journal of Geophysical Research*, *105*(A6), 13,089–13,101. https://doi.org/10.1029/1999JA005089

Goldreich, P., & Farmer, A. J. (2007). Spontaneous axisymmetry breaking of the external magnetic field at Saturn. *Journal of Geophysical Research*, *112*, A05225. https://doi.org/10.1029/2006JA012163

Gurnett, D. A., Groene, J. B., Averkamp, T. F., Kurth, W. S., Ye, S.-Y., & Fischer, G. (2011). An SLS4 longitude system based on a tracking filter analysis of the rotational modulation of Saturn kilometric radiation. *Planetary Radio Emissions*, *7*, 51–64. https://doi.org/10.1553/PRE7s51

Gurnett, D. A., Kurth, W. S., Hospodarsky, G. B., Persoon, A. M., Averkamp, T. F., Cecconi, B., et al. (2005). Radio and plasma wave observations at Saturn from Cassini's approach and first orbit. *Science*, *307*(5713), 1255–1259. https://doi.org/10.1126/science.1105356

Gurnett, D. A., Lecacheux, A., Kurth, W. S., Persoon, A. M., Groene, J. B., Lamy, L., et al. (2009). Discovery of a north-south asymmetry in Saturn's radio rotation period. *Geophysical Research Letters*, *36*, L16102. https://doi.org/10.1029/2009GL039621

Gurnett, D. A., Persoon, A. M., Groene, J. B., Kopf, A. J., Hospodarsky, G. B., & Kurth, W. S. (2009). A north-south difference in the rotation rate of auroral hiss at Saturn: Comparison to Saturn's kilometric radio emission. *Geophysical Research Letters*, *36*, L21108. https://doi.org/10.1029/2009GL040774

Gurnett, D. A., Persoon, A. M., Kurth, W. S., Groene, J. B., Averkamp, T. F., Dougherty, M. K., & Southwood, D. J. (2007). The variable rotation period of the inner region of Saturn's plasma disk. *Science*, *316*(5823), 442–445. https://doi.org/10.1126/science.1138562

Hill, T. W. (2016). Penetraing of external plasma into a rotation-driven magnetosphere. *Journal of Geophysical Research: Space Physics*, *121*, 10,032–10,036. https://doi.org/10.1002/2016JA023430

Hill, T. W., Rymer, A. M., Burch, J. L., Crary, F. J., Young, D. T., Thomsen, M. F., et al. (2005). Evidence for rotationally driven plasma transport in Saturn's magnetosphere. *Geophysical Research Letters*, *32*, L14S10. https://doi.org/10.1029/2005GL022620

Hunt, G. J., Cowley, S. W. H., Provan, G., Bunce, E. J., Alexeev, I. I., Belenkaya, E. S., et al. (2014). Field-aligned currents in Saturn's southern nightside magnetosphere: Subcorotation and planetary period oscillation components. *Journal of Geophysical Research: Space Physics*, *119*, 9847–9899. https://doi.org/10.1002/2014JA020506

Hunt, G. J., Cowley, S. W. H., Provan, G., Bunce, E. J., Alexeev, I. I., Belenkaya, E. S., et al. (2015). Field-aligned currents in Saturn's northern nightside magnetosphere: Evidence for interhemispheric current flow associated with planetary period oscillations. *Journal of Geophysical Research: Space Physics*, *120*, 7552–7584. https://doi.org/10.1002/2015JA021454

Jia, X., & Kivelson, M. G. (2012). Driving Saturn's magnetospheric periodicities from the upper atmosphere/ionosphere: Magnetotail response to dual sources. *Journal of Geophysical Research*, *117*, A11219. https://doi.org/10.1029/2012JA018183

Jia, X., Kivelson, M. G., & Gombosi, T. I. (2012). Driving Saturn's magnetospheric periodicities from the upper atmosphere/ionosphere. *Journal of Geophysical Research*, *117*, A04215. https://doi.org/10.1029/2011JA017367

Kennelly, T. J., Leisner, J. S., Hospodarsky, G. B., & Gurnett, D. A. (2013). Ordering of injection events within Saturnian SLS longitude and local time. *Journal of Geophysical Research: Space Physics*, *118*, 832–838. https://doi.org/10.1002/jgra.50152

Khurana, K. K., Mitchell, D. G., Arridge, C. S., Dougherty, M. K., Russell, C. T., Paranicas, C., et al. (2009). Sources of rotational signals in Saturn's magnetosphere. *Journal of Geophysical Research*, *114*, A02211. https://doi.org/10.1029/2008JA013312

Kollmann, P., Roussos, E., Kotova, A., Paranicas, C., & Krupp, N. (2017). The evolution of Saturn's radiation belts modulated by changes in radial diffusion. *Nature Astronomy*, *1*(12), 872–877. https://doi.org/10.1038/s41550-017-0287-x

Komori, A., Sato, N., & Hatta, Y. (1978). Excitation and control of the Rayleigh-Taylor instability in a plasma with a curved magnetic field. *Physical Review Letters*, *40*(12), 768–771. https://doi.org/10.1103/PhysRevLett.40.768

Krimigis, S. M., Mitchell, D. G., Hamilton, D. C., Livi, S., Dandouras, J., Jaskulek, S., et al. (2004). Magnetosphere Imaging Instrument (MIMI) on the Cassini mission to Saturn/Titan. *Space Science Reviews*, *114*(1–4), 233–329. https://doi.org/10.1007/s11214-004-1410-8

Kurth, W. S., Averkamp, T. F., Gurnett, D. A., Groene, J. B., & Lecacheux, A. (2008). An update to a Saturnian longitude system based on kilometric radio emissions. *Journal of Geophysical Research*, *113*, A05222,. https://doi.org/10.1029/2007JA012861

Lai, H. R., Russell, C. T., Jia, Y. D., Wei, H. Y., & Dougherty, M. K. (2016). Transport of magnetic flux and mass in Saturn's inner magnetosphere. *Journal of Geophysical Research: Space Physics*, *121*, 790–803. https://doi.org/10.1002/2015JA021980

Lamy, L. (2017). The Saturnian kilometric radiation before the Cassini Grand Finale. In G. Fischer, G. Mann, M. Panchenko, & P. Zarka (Eds.), *Planetary radio emissions* (Vol. 8, pp. 171–190).

Liu, X., Hill, T. W., Wolf, R. A., Sazykin, S., Spiro, R. W., & Wu, H. (2010). Numerical simulation of plasma transport in Saturn's inner magnetosphere using the Rice convection model. *Journal of Geophysical Research*, *115*, A12254. https://doi.org/10.1029/2010JA015859

Nichols, J. D., Cecconi, B., Clarke, J. T., Cowley, S. W. H., Gérard, J.-C., Grocott, A., et al. (2010). Variation of Saturn's UV aurora with SKR phase. *Geophysical Research Letters*, *37*, L15102. https://doi.org/10.1029/2010GL044057

Paranicas, C., Mitchell, D. G., Roelof, E. C., Brandt, P. C., Williams, D. J., Krimigis, S. M., & Mauk, B. H. (2005). Periodic intensity variations in global ENA images of Saturn. *Geophysical Research Letters*, *32*, L21101. https://doi.org/10.1029/2005GL023656

Paranicas, C., Thomsen, M. F., Achilleos, N., Andriopoulou, M., Badman, S. V., Hospodarsky, G., et al. (2016). Effects of radial motion on interchange njections at Saturn. *Icarus*, *264*, 342–351. https://doi.org/10.1016/j.icarus.2015.10.002

Porco, C. C., & Danielson, G. E. (1982). The periodic variation of spokes in Saturn's rings. *The Astronomical Journal*, *87*(5), 826. https://doi.org/10.1086/113162

Provan, G., Andrews, D. J., Arridge, C. S., Coates, A. J., Cowley, S. W. H., Cox, G., et al. (2012). Dual periodicities in planetary-period magnetic field oscillations in Saturn's tail. *Journal of Geophysical Research*, *117*, A01209. https://doi.org/10.1029/2011JA017104

Provan, G., Andrews, D. J., Arridge, C. S., Coates, A. J., Cowley, S. W. H., Milan, S. E., et al. (2009). Polarization and phase of planetary-period magnetic field oscillations on high-latitude field lines in Saturn's magnetosphere. *Journal of Geophysical Research*, *114*, A02225. https://doi.org/10.1029/2008JA013782

Provan, G., Cowley, S. W. H., Bradley, T. J., Bunce, E. J., Hunt, G. J., & Dougherty, M. K. (2018). Planetary period oscillations in Saturn's magnetosphere: Cassini magnetic field observations over the northern summer solstice interval. *Journal of Geophysical Research: Space Physics*, *123*, 3859–3899. https://doi.org/10.1029/2018JA025237

Provan, G., Cowley, S. W. H., Lamy, L., Bunce, E. J., Hunt, G. J., Zarka, P., & Dougherty, M. K. (2016). Planetary period oscillations in Saturn's magnetosphere: Coalescence and reversal of northern and southern periods in late northern spring. *Journal of Geophysical Research: Space Physics*, *121*, 9829–9862. https://doi.org/10.1002/2016JA023056

Provan, G., Cowley, S. W. H., Sandhu, J., Andrews, D. J., & Dougherty, M. K. (2013). Planetary period magnetic field oscillations in Saturn's magnetosphere: Post equinox abrupt nonmonotonic transitions to northern system dominance. *Journal of Geophysical Research: Space Physics*, *118*, 3243–3264. https://doi.org/10.1002/jgra.50186

Provan, G., Lamy, L., Cowley, S. W. H., & Dougherty, M. K. (2014). Planetary period oscillations in Saturn's magnetosphere: Comparison of magnetic oscillations and SKR modulations in the post equinox interval. *Journal of Geophysical Research: Space Physics*, *119*, 7380–7401. https://doi.org/10.1002/2014JA020011

Ramer, K. M., Kivelson, M. G., Sergis, N., Khurana, K. K., & Jia, X. (2017). Spinning, breathing, and flapping: Periodicities in Saturn's middle magnetosphere. *Journal of Geophysical Research: Space Physics*, *122*, 393–416. https://doi.org/10.1002/2016JA023126

Roussos, E., Krupp, N., Paranicas, C., Carbary, J. F., Kollmann, P., Krimigis, S. M., & Mitchell, D. G. (2014). The variable extension of Saturn's electron radiation belts. *Planetary and Space Science*, *104*, 3–17. https://doi.org/10.1016/j.pss.2014.03.021

Rymer, A. M., Mauk, B. H., Hill, T. W., André, N., Mitchell, D. G., Paranicas, C., et al. (2009). Cassini evidence for rapid interchange transport at Saturn. *Planetary and Space Science*, *57*(14–15), 1779–1784. https://doi.org/10.1016/j.pss.2009.04.010

Seidelmann, P. K., & Divine, N. (1977). Evaluation of Jupiter longitudes in system III (1965). *Geophysical Research Letters*, *4*(2), 65–68. https://doi.org/10.1029/GL004i002p00065

Sergis, N., Jackman, C. M., Thomsen, M. F., Krimigis, S. M., Mitchell, D. G., Hamilton, D. C., et al. (2017). Radial and local time structure of the Saturnian ring current, revealed by Cassini. *Journal of Geophysical Research: Space Physics*, *122*, 1803–1815. https://doi.org/10.1002/2016JA023742

Shain, C. A. (1955). Location on Jupiter of a source of radio noise. *Nature*, *176*(4487), 836–837. https://doi.org/10.1038/176836a0

Smith, C. G. A. (2006). Periodic modulation of gas giant magnetospheres by the neutral upper atmosphere. *Annales Geophysicae*, *24*(10), 2709–2717. https://doi.org/10.5194/angeo-24-2709-2006

Southwood, D. J., & Cowley, S. W. H. (2014). The origin of Saturn's magnetic periodicities: Northern and southern current systems. *Journal of Geophysical Research: Space Physics*, *119*, 1563–1571. https://doi.org/10.1002/2013JA019632

Southwood, D. J., & Kivelson, M. G. (1987). Magnetospheric interchange instability. *Journal of Geophysical Research*, *92*(A1), 109–116. https://doi.org/10.1029/JA092iA01p00109

Southwood, D. J., & Kivelson, M. G. (1989). Magnetospheric interchange motions. *Journal of Geophysical Research*, *94*(A1), 299–308. https://doi.org/10.1029/JA094iA01p00299

Stevenson, D. J. (2006). A new spin on Saturn. *Nature*, *441*(7089), 34–35. https://doi.org/10.1038/441034a

Thomsen, M. F. (2013). Saturn's magnetospheric dynamics. *Geophysical Research Letters*, *40*, 5337–5344. https://doi.org/10.1002/2013GL057967

Thomsen, M. F., Coates, A. J., Roussos, E., Wilson, R. J., Hansen, K. C., & Lewis, G. R. (2016). Suprathermal electron penetration into the inner magnetosphere of Saturn. *Journal of Geophysical Research: Space Physics*, *121*, 5436–5448. https://doi.org/10.1002/2016JA022692

Thomsen, M. F., Reisenfeld, D. B., Delapp, D. M., Tokar, R. L., Young, D. T., Crary, F. J., et al. (2010). Survey of ion plasma parameters in Saturn's magnetosphere. *Journal of Geophysical Research*, *115*, A10220. https://doi.org/10.1029/2010JA015267

Wilson, R. J., Bagenal, F., & Persoon, A. M. (2017). Survey of thermal plasma ions in Saturn's magnetosphere utilizing a forward model. *Journal of Geophysical Research: Space Physics*, *122*, 7256–7278. https://doi.org/10.1002/2017JA024117

Ye, S. Y., Fischer, G., Kurth, W. S., Menietti, J. D., & Gurnett, D. A. (2016). Rotational modulation of Saturn's radio emissions after equinox. *Journal of Geophysical Research: Space Physics*, *121*, 11,714–11,728. https://doi.org/10.1002/2016JA023281

Ye, S.-Y., Fischer, G., Kurth, W. S., Menietti, J. D., & Gurnett, D. A. (2018). An SLS5 longitude system based on the rotational modulation of Saturn radio emissions. *Geophysical Research Letters*, *45*, 7297–7305. https://doi.org/10.1029/2018GL077976

Yu, Z. J., & Russell, C. T. (2009). Rotation period of Jupiter from the observation of its magnetic field. *Geophysical Research Letters*, *36*, L20202. https://doi.org/10.1029/2009GL040094